

Rock-Type Definition and Pore Characterization of Tight Carbonate Rocks Based on Thin Sections and MICP and NMR Experiments

Fei Tian¹ · Weimin Wang² · Naigui Liu¹ · Jiaqi Jiang² · Congkai Niu³ · Yuandong Zhang² · Yaxi Li³

Received: 26 September 2017 / Revised: 23 January 2018 / Published online: 27 March 2018
© Springer-Verlag GmbH Austria, part of Springer Nature 2018

Abstract Thick tight Ordovician carbonate rocks are present at depths exceeding 5300 m in the Tahe oilfield and their matrix is considered to contain no storage space. An integrated petrographical and petrophysical study was conducted on a set of 25 tight carbonate core samples from Ordovician strata, covering a wide range of lithologies and textures. Six carbonate rock types were characterized by integrating both petrographical and petrophysical data, including thin-section observations and porosity, permeability, mercury injection capillary pressure and nuclear magnetic resonance (NMR) measurements. We found that thick grainstone and limestone with half-filled fractures exhibited good reservoir properties. NMR testing is an invaluable tool for characterizing pore structures in tight carbonate rocks. For example, six rock types can be identified from the NMR T_2 distributions and the changes in pore volume under different pressures (up to 20 MPa) can be calculated. NMR technology can be used to perform rapid and accurate rock-type identification and pore network evaluation in tight carbonate rocks. The results provide an experimental foundation for NMR logging interpretations and advance the understanding of geological and geophysical characteristics of ultra-deep carbonate reservoirs.

✉ Weimin Wang
wmw@pku.edu.cn

¹ Key Laboratory of Petroleum Resources Research, Institute of Geology and Geophysics, Chinese Academy of Sciences, Beijing 100029, China

² Institute of Quantum Electronics of Peking University, Beijing 100871, China

³ College of Geosciences, China University of Petroleum, Beijing 102249, China

1 Introduction

Oil and gas production from carbonate reservoirs, an important oil and gas reservoir type, accounts for more than 63% of the total hydrocarbon output of the world, and approximately 70% of oil reserves and 90% of gas reserves in the Middle East are located in carbonate reservoirs [1]. The marine carbonate sedimentary deposition area in China is large ($250 \times 10^4 \text{ km}^2$) and rich in oil and gas resources [2]. As large carbonate oil and gas fields continue to be discovered, such as in the Tarim, Sichuan, and Bohai Bay basins, carbonate reservoirs have become an important aspect of the hydrocarbon resources in China [3]. The Tahe oilfield, located in the northern uplift of the Tarim Basin, is the largest Paleozoic marine carbonate oilfield in China. The main hydrocarbon storage space is Ordovician paleocaves and related fractures with burial depths of more than 5300 m [4]. The host carbonates and paleocaves have undergone a variety of geological processes, such as karstification, burial, collapse and filling, that have led to generally poor physical reservoir properties [5]. The distribution of paleokarst reservoirs was delineated using seismic datasets [4, 6, 7]. Jin et al. [8, 9] and Lu et al. [5] discussed the relationship between paleokarst fill and oil and gas production. However, in some parts of the Tahe oilfield, the volume extracted during current oil and gas production is greater than the volume of the paleocaves delineated by seismic data, suggesting that considerable storage space exists outside the paleocaves. It is unclear whether the host rocks are reservoirs or potential hydrocarbon migration pathways. Considering the strong heterogeneity present in carbonate rocks, the physical properties of carbonate host rocks depend largely on the characteristics of their pore structures. Detailed characterizations of the pore structure in such deeply buried host rocks have very important theoretical and practical implications.

In recent years, the nature of the pore structure in carbonate rocks has attracted more attention. Many new technologies, such as the scanning electron microscope (SEM), nuclear magnetic resonance (NMR) technology, and computed tomography (CT), have been used in laboratory experiments. NMR has been widely used due to its accurate, rapid and nondestructive evaluation of core samples [10]. Following the initial development of NMR, Mariappan et al. [11] suggested improvements of the experimental methods for this technique. Ge et al. [12], Claverie et al. [13], and Deng et al. [14] divided carbonate pore structures into different types using NMR response characteristics. Farooq et al. [15] and Li [16] analyzed the relationship between porosity and permeability in carbonate reservoirs using NMR T_2 spectra. Furthermore, Vik et al. [17] and Rezende et al. [18] used NMR to analyze the pore connectivity of carbonate reservoirs. However, most of the studies mentioned above focused on porous carbonate reservoirs. There are few published studies on the characterization of tight carbonate rocks using NMR experiments, especially for the deeply buried tight carbonate rocks in the Tahe oilfield.

To define the pore structure characteristics of deeply buried tight carbonate rocks in the Tahe oilfield, 25 typical core samples were selected from sections

without paleokarst development. Based on core sample and thin-section observations, mercury injection capillary pressure (MICP) profiles and NMR characteristics, the petrographical characteristics of the samples were identified, and the petrophysical characteristics of these samples, including their porosity and permeability, were assessed. The NMR characteristics of the samples were measured under both atmospheric pressure and overburden pressure conditions (up to 20 MPa). Based on the petrographical and petrophysical characteristics, a comprehensive petrographical–petrophysical analysis was conducted to characterize the pore structure of the deeply buried tight carbonate rocks in the Tahe oilfield. The results provide an experimental foundation for NMR logging interpretations and advance the understanding of geological and geophysical characteristics of deep carbonate reservoirs.

2 Materials and Methods

2.1 Sampling

The Ordovician strata in the Tahe oilfield experienced multiple stages of karstification during the late Hercynian and early Caledonian periods, resulting in the formation of complex paleokarst systems [4, 18, 19]. Samples were collected from the Yingshan Formation in six typical wells. This paper focuses on the petrographical and petrophysical properties of the tight carbonate rocks rather than the paleokarst sections. According to the needs of this study, cores were sampled by carefully avoiding paleokarst zones (e.g., caves and fractures around caves). Considering the carbonate heterogeneity, the samples were taken from homogeneous sections with lengths of at least 30 cm. The 25 core samples were collected from tight limestone sections that had not been affected by karstification. Therefore, the core samples in this study are tight carbonate rocks and do not show evidence of karstification. These samples were made into cylinders 2.45–2.53 cm in diameter and 3.72–5.05 cm in length.

2.2 Petrography

In this study, we created 30- μm -thick thin sections. Based on detailed observations of these thin sections and the Dunham carbonate classification, the microscopic sedimentary characteristics of the samples were identified, and their rock types were classified into mudstone, wackestone, packstone and grainstone, with a particle size limit for mud of 30 μm . For the limestone samples with fractures, two classifications were added: limestone with half-filled fractures and limestone with fully filled fractures. In the limestone samples with half-filled fractures, the fractures are mainly filled with calcite and have widths of 0.2–1 mm. In the limestone samples with fully filled fractures, the fractures are relatively narrow and have widths of less than 0.3 mm.

2.3 Petrophysics

2.3.1 Porosity and permeability

In this paper, the porosity and permeability of 25 core samples are measured. The porosity was determined using nitrogen adsorption and a continuous flow method to determine grain volume and bulk volume based on Boyle's law of isothermal expansion [20]. The permeability of core samples was determined by Darcy's law, which reflects the ability of a fluid to pass through the rock sample under a pressure difference [21]. The transfer "down" principle was used to measure permeability in this study. Helium was used in the core-flooding experiment, in which a known volume flows through the samples and into the atmosphere, and the flooding pressure attenuation was monitored over time. For each given time, the gas flow velocity and pressure drop in the rock can be determined, and the permeability can then be determined by calculating the changes in inlet pressure over time.

2.3.2 Mercury injection capillary pressure (MICP)

Microscope observations of thin sections and image analysis of pores can be used to directly observe the shape, size, and connectivity of pores and pore throats in a planar view, but these methods cannot be used to qualitatively or quantitatively evaluate a three-dimensional pore throat system. When porous channels have many twists and turns, the resulting pore throat system in a tight carbonate rocks is very complex, and thin-section observations show only part of the pore throat system. Mercury injection capillary pressure (MICP) testing involves injecting mercury as a non-wetting phase into the pore system to overcome the capillary pressure formed by the pores and pore throats. The mercury injection pressure and volume can then be used to find the relationship between pressure and mercury saturation [22]. The mercury injection capillary pressure curve reflects the pore throat structure and its probability distribution and can be used to characterize the pore structure parameters of core samples, such as the mean number of pore throats, pore throat sorting coefficient, and average pore throat radius. Additionally, the shape of the capillary pressure curve depends on the connectivity of the pores and the size distribution of the pores, and in conjunction with the NMR method, a quantitative characterization of the pore structure can be achieved.

2.3.3 Nuclear magnetic resonance (NMR)

The principles of the NMR method are described in detail in [23–25]. NMR is a powerful tool for characterizing the pore size distribution using the magnetization decay of fluid molecules. According to the NMR theory and NMR relaxation mechanism, the NMR T_2 spectra of a saturated single-phase fluid (water is generally used) can reflect the internal pore structure.

$$\frac{1}{T_2} = \frac{1}{T_{2B}} + \rho_2 \left(\frac{S}{V} \right) + \frac{D(\gamma G T_E)^2}{12}, \quad (1.1)$$

where T_{2B} is the volume (freedom) relaxation time of the fluid, ms; D is the diffusion coefficient, $\mu\text{m}^2/\text{ms}$; G is the magnetic gradient, Gs/cm; T_E is the echo interval, ms; S is the pore surface area, cm^2 ; V is the pore volume, cm^3 ; and ρ_2 is the transverse surface relaxation strength of the rock, $\mu\text{m}/\text{ms}$, which is a parameter related to the properties of the rock and is not affected by pressure and temperature.

T_{2B} is usually in the range of 2000–3000 ms, which is much longer than T_2 , that is, $T_{2B} \gg T_2$; thus, $\frac{1}{T_{2B}}$ can be ignored. G is very small when the magnetic field is uniform, and $\frac{D(\gamma GT_E)^2}{12}$ can be ignored when T_E is very short. In this case, the transverse relaxation time is directly related to the specific surface $\frac{S}{V}$ of the pores. Thus, the previous equation can be simplified as follows:

$$\frac{1}{T_2} = \rho_2 \left(\frac{S}{V} \right). \quad (1.2)$$

Equation 1.2 shows that for intergranular pore-dominated rocks, the T_2 size is mainly determined by the lithology (ρ_2) and pore ratio $\left(\frac{S}{V} \right)$. If the pore is an ideal sphere, $\frac{S}{V} = \frac{3}{r_c}$, and if the pore is an ideal cylinder, $\frac{S}{V} = \frac{2}{r_c}$. If the aperture radius is proportional to the throat radius, Eq. 1.2 can be rewritten as follows:

$$\frac{1}{T_2} = \rho_2 \left(\frac{F_S}{r_c} \right), \quad (1.3)$$

where F_S is the pore shape factor.

In NMR experiments, the pore radius (r_c) is proportional to T_2 . In sample cylinders with small pores, most of the fluid is in a restrained state, and there is little movable fluid; hence, the relaxation time is short and plots mainly on the left part of the T_2 spectrum. In sample cylinders with large or medium pores, or even fractures, there is more movable fluid, and the fluid relaxation time is longer and plots mainly on the right part of the T_2 spectrum.

2.3.4 NMR Online Test System

Using a laboratory NMR experiment to measure the T_2 distribution has many advantages, such as a high degree of automation, simple operation procedure, short run time, and no damage to rock samples. Hence, this method is suitable for the study of the pore structures of multiple core sample types. The experimental apparatus used in this study is a high-temperature and high-pressure online test platform at the Institute of Geology and Geophysics, Chinese Academy of Sciences. The experimental set-up is mainly composed of a SPEC-023-B NMR core analyser (Beijing Spike Technology Development Co., Ltd.), a TEL-EDYNE ISCO pump, a ring pressure pump and a non-metallic, non-magnetic core holder (Fig. 1). The magnetic field strength of the NMR analyser is 0.23 T,

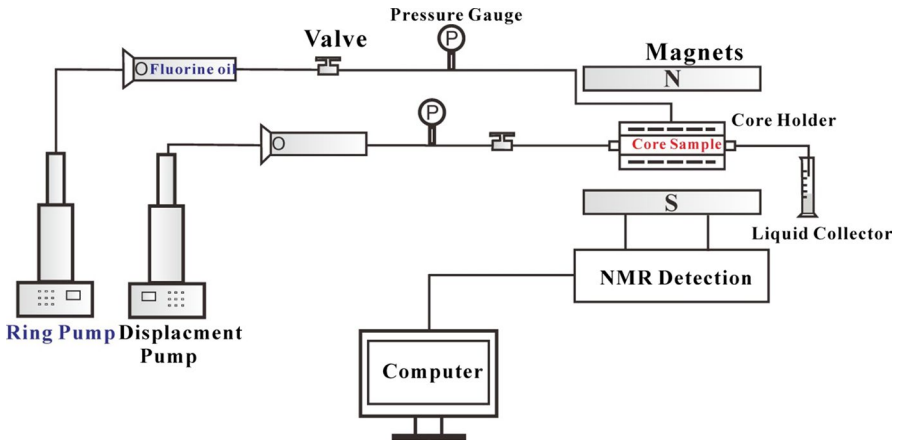


Fig. 1 System structure of the NMR online testing instrument

and the magnet net space is 330 mm. The detection coil uses a transmitting and receiving common coil with an inner diameter of 280 mm. In the experiment, the Carr–Purcell–Meiboom–Gill (CPMG) measurement sequence was used [26]. The parameters were as follows: the resonant frequency was 10.11 MHz, the echo time was 150 μ s, the number of accumulated scans was 16, the sampling interval was 1 μ s, and the echo number was 8192. The core holder is made of polyetheretherketone (PEEK) material, which aids in the calculation of the displacement during the NMR online measurements. The core holder is pressurized at a pre-set ring pressure by the ring pressure system to simulate the in situ formation pressure, and a hydrogen-free perfluorocarbon oil is used as a toroidal fluid. The TELEDYNE ISCO pump ensures that the fluid is displaced into the core when the fluid is under constant flow or constant pressure. Computer terminals collect the core data in a T_2 relaxation time spectrum using special software, and the experimental data are saved online.

3 Results

3.1 Petrography

Based on the integration of both the petrographical observations and the NMR measurements, six rock types were defined: (1) mudstone, (2) wackestone, (3) packstone, (4) grainstone, (5) limestone with half-filled fractures and (6) limestone with fully filled fractures (see overview of petrographical observations in Fig. 2 and petrophysical results in Fig. 3 and Table 1).

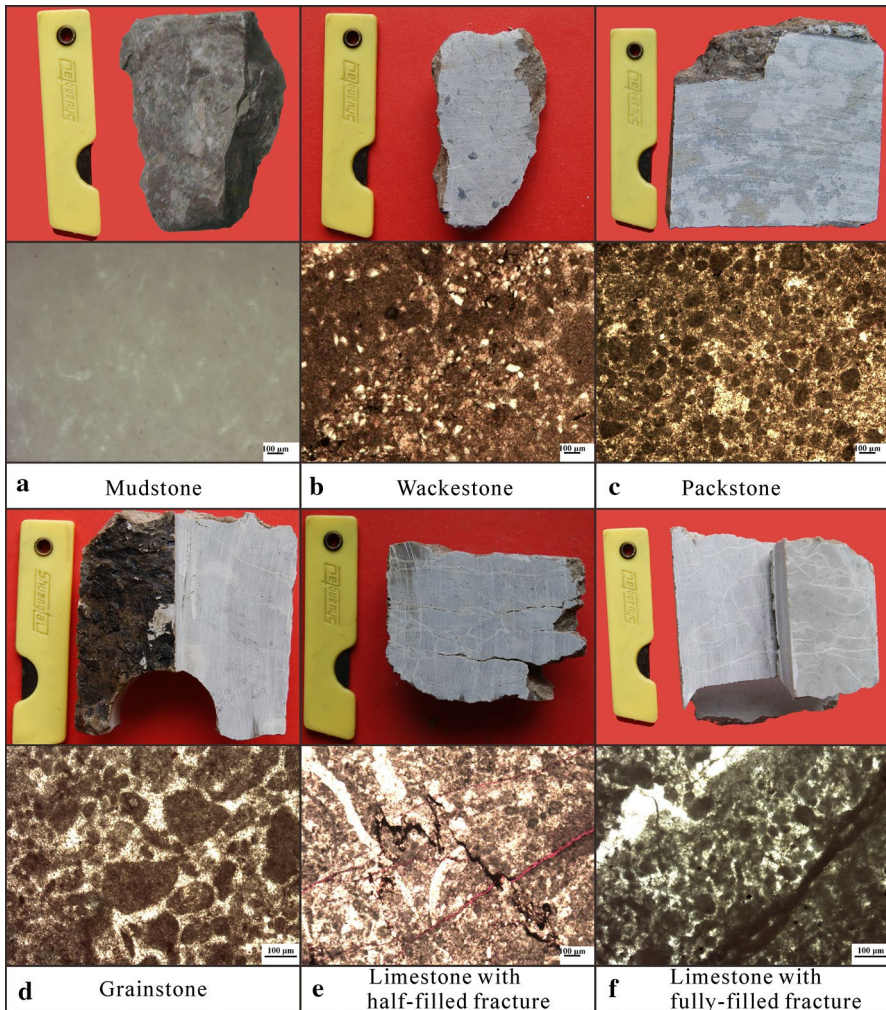
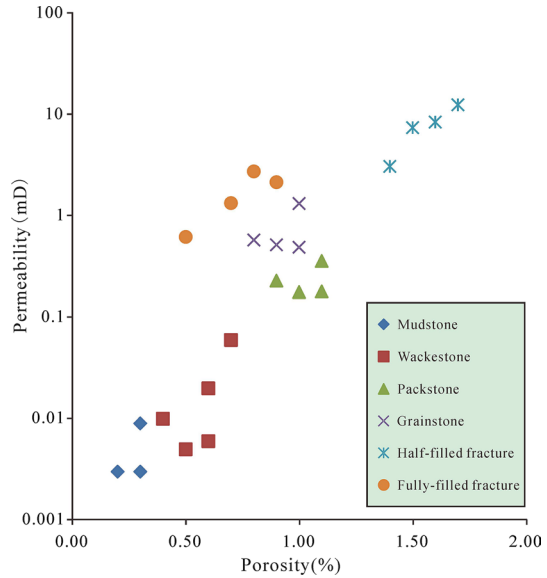


Fig. 2 Core and thin sections images from the tight carbonate in the Tahe oilfield. **a** Mudstone, **b** wackestone, **c** packstone, **d** grainstone, **e** limestone with half-filled fractures, **f** limestone with fully filled fractures

3.1.1 Mudstone

Mudstone is a muddy carbonate rock containing less than 10% grains. The term mudstone is synonymous with calcilutite, except that it does not specify the mineralogical composition and thus avoids such ambiguities as dolomite calcilutite. The significance of mudstone, aside from the implication of calm water during deposition, is the apparent lack of grain-producing organisms [27]. Mudstone forms in calm hydrodynamic conditions and appears in lagoons, depressions, lime mud mounds and interbank sea depositional subfacies. The mudstone in this

Fig. 3 Porosity and permeability of the core samples



study is very tight and dark gray in color (Fig. 1a). The thin-section observations reveal no dissolution phenomena, and the mudstone lacks effective pores.

3.1.2 Wackestone

Mud-supported carbonate rocks containing more than 10 per cent grains are called wackestones. Wackestone forms on the gentle slope of platforms and in intraplatform depositional subfacies and is mainly composed of mud with some particles. The cores show that the wackestone is mostly gray with black spots (Fig. 2b). The thin sections show that it is composed mainly of muddy carbonate with some suspended carbonate grains.

3.1.3 Packstone

Grain-supported muddy carbonate rocks are called packstones. Grain support is generally a property of rocks deposited in agitated water, whereas muddiness is generally a property of rocks deposited in quiet water; packstone is a mixture of these two sedimentary environments and often forms in sedimentary subfacies associated with the platforms of internal reefs or grain shoals. The packstone in the cores is a grayish white color with dark patches. White calcite cements can be observed between the grains, and there is also some dark mud forming a matrix between the particles (Fig. 2c).

Table 1 Geometry, density, porosity and permeability of the samples

Rock type	Sample number	Depth (m)	Length (cm)	Diameter (cm)	Porosity (%)	Permeability (mD)
Mudstone	1	5681.89	4.37	2.45	0.21	0.003
	2	5365.06	4.15	2.52	0.32	0.003
	3	5679.52	4.26	2.53	0.34	0.009
Wackestone	4	5386.64	4.13	2.53	0.63	0.02
	5	5387.31	4.29	2.46	0.72	0.06
	6	5389.56	4.53	2.52	0.59	0.006
	7	5390.41	4.41	2.53	0.38	0.01
	9	5392.47	4.33	2.53	0.51	0.005
Packstone	11	5394.34	4.42	2.52	0.42	0.01
	13	5385.47	4.45	2.53	0.93	0.23
	15	5905.26	4.42	2.53	1.12	0.36
	16	5789.17	3.72	2.52	1.09	0.18
Grainstone	17	5433.37	5.05	2.48	1.02	0.177
	18	5702.09	4.39	2.53	1.01	0.49
	19	5737.12	3.95	2.52	0.92	0.52
	20	5887.29	4.38	2.53	0.81	0.58
	21	5897.13	4.46	2.53	1.03	1.33
Limestone with half-filled fractures	30	5556.66	4.42	2.53	1.41	3.08
	31	5725.95	4.53	2.53	1.63	8.45
	32	5727.37	4.37	2.48	1.54	7.46
	33	5891.97	4.29	2.53	1.71	12.5
Limestone with fully-filled fractures	23	5812.51	4.41	2.52	0.53	0.62
	24	5810.31	4.99	2.53	0.91	2.16
	25	5811.48	4.11	2.53	0.69	1.34
	26	5753.79	4.35	2.53	0.81	2.76

3.1.4 Grainstone

Grainstone is the term given to grain-supported, mud-free carbonate rocks. The grains are mainly composed of intraclasts, oolites and bioclasts. Grainstone usually forms in intraplatform and grain shoal sedimentary environments and is a product of highly hydrodynamic conditions. The grains and bright crystalline cements of grainstone are easily corroded, forming intragranular and intergranular dissolution pores. In this study, the cores contain mainly pure gray grainstone (Fig. 2d). The diameters of the grainstone grains in thin section range from 50 to 150 μm , and spar occurs locally between the grains.

3.1.5 Limestone with Half-Filled Fractures

In the tight carbonate zones, the development of fractures can improve the physical properties of reservoirs significantly. Dissolution, precipitation and other diagenetic interactions are common, resulting in a strong heterogeneity in the degree of fracture filling. The fractures in the cores are mainly horizontal fractures, and some unfilled fractures can also be distinguished with the naked eye (Fig. 2e). Several unfilled fractures can be found in the thin sections (the red lines in Fig. 2e indicate open fractures).

3.1.6 Limestone with Fully Filled Fractures

Fractures can become fully filled due to calcite precipitation when the subsurface water within the fractures is stagnant. In this study, the fractures that are fully filled with limestone are mostly horizontal fractures with narrow widths (< 0.3 mm). The material filling the fractures is mainly calcite (Fig. 2f).

3.2 Petrophysics

3.2.1 Porosity and Permeability

In this paper, the porosity of the limestone is 0.2–2%, and the permeability is 0.003–12.5 mD (Fig. 3, Table 1). The porosity of the tight limestone of the six rock types clearly varies. The porosity of the mudstone is less than 0.5%, and the porosity of the grainstone and packstone is 0.92–1.12%. However, fractures can significantly improve the permeability of the limestone. Although the porosity of the fully filled fractures is 0.53–0.91%, the permeability (0.62–2.76 mD) is higher than that of the tight limestone. Half-filled fractures have high porosity and permeability values, with the porosity and permeability reaching peak values of 1.71% and 12.5 mD, respectively (Fig. 3).

3.2.2 MICP

Storage space is the basic characteristic of a carbonate reservoir. Impacted by compaction, diagenesis and tectonic activity, the pore structure of deeply buried tight carbonate rocks is much more complicated than that of sandstones in shallow formations. If the pores and pore throats are large enough to be visible to the naked eye, these systems can be identified by observations. The carbonate grain and pore throat sizes can be observed with 100 times magnification (Fig. 2); hence, it is not possible to estimate the rock type and pore geometry with the naked eye. The mercury curve effectively reflects the pore structure of the cylinders, and the shape of the curve is mainly controlled by the separation of the pore volume and pore throat size. The slope of the capillary pressure test curve reflects the volume percentage of the fluid entering the pore, under a certain capillary

pressure (P_c), through a pore throat of a specific size. For specific rock types, the capillary pressure curve represents a petrophysical description that can be used to characterize the pore structure of tight carbonate rocks. To analyze the reservoir property using the capillary pressure curve, 25 capillary pressure curves

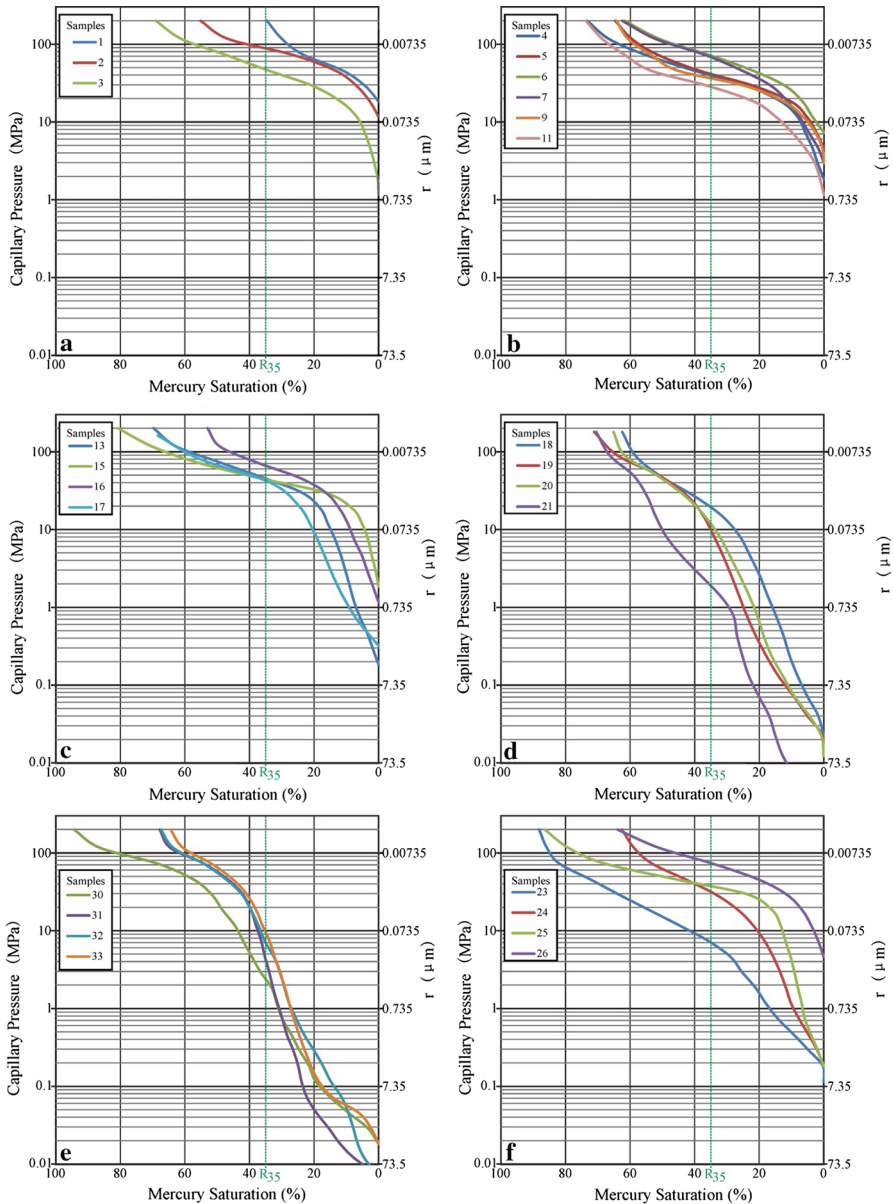


Fig. 4 MICP curves for the sample cylinders. **a** Mudstone, **b** wackestone, **c** packstone, **d** grainstone, **e** limestone with half-filled fractures, **f** limestone with fully filled fractures

belonging to six rock types were measured (Fig. 4), and three types of pore throat systems were identified.

3.2.2.1 Pore Throat System I The mudstone and wackestone are mud-supported carbonate rocks, and they belong to pore throat system I. This pore throat system is dominated by pore throats, has poor pore connectivity and a large mercury seepage resistance. The displacement pressure of the mudstone can exceed 10 MPa (Fig. 4a), and the displacement pressure of wackestone is greater than 1 MPa (Fig. 4b). The average throat diameter is determined by the smoothest part of the mercury curve, and Pittman et al. proposed that the mercury curve R_{35} represents the typical pore throat radius of the rock sample [28]. The mercury curve profiles show that the mud-supported limestone has the most obvious pressure mercury plateaus (approximately 20–40 MPa), and the corresponding pore throat radius is approximately 18–36 nm. Sample reservoir performance is determined by the steep section on the left side of the mercury injection curve. For pore throat system I, the volume percentage is approximately 10%, suggesting that this pore throat system may not form good oil and gas reservoirs.

3.2.2.2 Pore Throat System II The packstone and grainstone are grain-supported carbonate rocks, and they belong to pore throat system II. According to the mercury injection data, this type of pore throat system has better reservoir properties than system I. The displacement pressure of the packstone is less than 1 MPa (Fig. 4c), and the displacement pressure of the grainstone can reach 0.01 MPa (Fig. 4d). The mercury injection curves show that the grain-supported carbonate rocks have the distinct characteristic of two steep sections. The volume per cent of the right steep section (small pore size) is approximately 20–30%, indicating a thick layer of high-porosity particle-supported limestone favorable for oil and gas storage.

3.2.2.3 Pore Throat System III Limestone samples with half-filled fractures and fully filled fractures in the fractured limestone group belong to pore throat system III. This pore throat system typically exhibits a double slope characteristic in the mercury curve, clearly showing two types of pore structures. The mercury displacement pressure of the fractured limestone is generally low, less than 1 MPa and even 0.01 MPa. There is no obvious plateau characteristic in the mercury curve for the limestone with half-filled fractures, indicating that the distribution of pore and pore throat sizes is continuous, and the volume percentage of the steep section of the pressure mercury curve can reach 40–50% (Fig. 4e). In the limestone with fully filled fractures, the fracture fill is visible to the naked eye and lacks effective connectivity among large pores, and the volume percentage of the right steep section on the mercury curve is approximately 20% (Fig. 4f).

3.2.3 NMR

T_2 is a characteristic time that represents the magnetic decay of the protons within a fluid after their polarization. The T_2 time of a single fluid-filled pore is proportional

to the volume to surface ratio (V/S) of the pore, which includes the pore shape factor and surface rugosity [22]. The logarithmic mean of the T_2 distribution (T_{2lm}) was calculated for each sample from the unimodal T_2 time distribution. The T_2 relaxation time spectrum is the distribution of different pore sizes in the sample. The T_2 relaxation time is proportional to the size of the pore radius, with longer relaxation times for larger pores. The results suggest that the NMR features of the six rock types vary significantly.

For mud-supported limestone (mudstone and wackestone), the NMR characteristics are a normal distribution with one peak. The mud-supported limestone NMR response and statistical peak position are shown in Fig. 5 and Table 2. Due to the pore sizes in the grain-supported limestone (packstone and grainstone) (Fig. 2c, d), the NMR has a peak on the left side of the response time axis, although the presence of some larger pores creates a certain response on the right side (> 200 ms for carbonate), which is especially obvious in the NMR results for the grainstone (Fig. 5b). The NMR responses of the limestone samples with half-filled and fully filled fractures (Fig. 5b). The NMR responses of the limestone samples with half-filled and fully

Fig. 5 The NMR T_2 distributions of each rock type. **a** Mud-supported limestone, including the mudstone and wackestone, **b** grain-supported limestone, including the packstone and grainstone, **c** fractured limestone, including the half-filled fractures and fully filled fractures

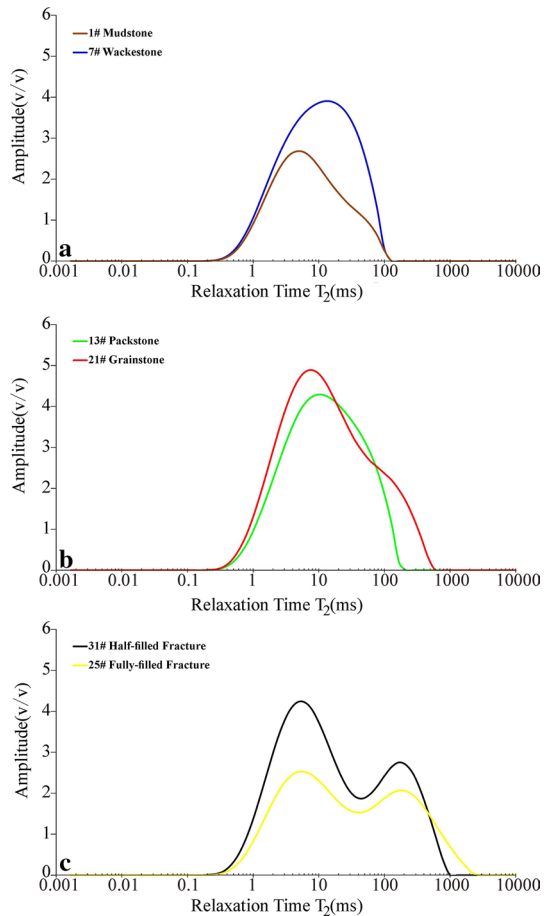


Table 2 NMR characteristics of different rock types

	Mudstone	Wackestone	Packstone	Grainstone	Limestone with half-filled fractures	Limestone with fully-filled fractures
Plug sample	1#	7#	13#	21#	31#	25#
Amplitude of peak (v/v)	4.85	13.38	9.67	7.53 (139.94)	5.21 (174.54)	5.17 (191.33)
T_2 of peak (ms)	2.67	3.89	4.29	4.89 (2.17)	4.23 (2.75)	2.53 (2.07)

filled fractures have clear bimodal peaks. Although some fractures appear filled to the naked eye, the NMR response shows that the fractures are also partially porous, possibly due to diagenesis (Fig. 5 and Table 2). According to the second peak on the NMR (Fig. 5c), we speculate that the limestone with half-filled fractures may have good-quality storage space.

To study the subsurface characteristics of the pore structure in tight carbonate rocks, NMR experiments were conducted under overburden conditions, with a pressure range of 2–20 MPa. Under increased pressure, some small changes were observed in the mudstone NMR curve shapes of the wackestone and packstone: the peak moved left (T_2 values decreased), and the amplitude decreased (Fig. 6a–c). The NMR curves of the grainstone are very interesting. Under pressures of 5–20 MPa, the volume of the mesopores increased (Fig. 6d). In other words, because the intergranular pores in the grainstone can be compacted under certain pressures, the macropores are compressed into mesopores, and the mesopores are compressed into micropores. The T_2 curve of the sample with half-filled fractures had the largest change, especially in the region of $T_2 > 200$ ms, and the pores were clearly compressed (Fig. 6e).

4 Discussion

Following an integrated analysis of the available petrographical and petrophysical data, including thin-section observations, rock-type identification, and porosity, permeability, MICP and NMR measurements, the NMR analysis appears to be an invaluable tool for characterizing tight carbonate pore structure. Six rock types can be identified from the NMR T_2 distributions; the volume percentages of micropores, mesopores and macropores can be calculated; and the changes in pore volume under different pressures (up to 20 MPa in this paper) can be calculated quantitatively. Consequently, NMR technology can be used to perform rapid and accurate rock-type identification and pore network evaluation on ultra-deep and tight carbonate rocks.

The spin–spin relaxation time T_2 value of the nuclear magnetic resonance is affected by many factors, such as the paramagnetic substance, temperature, pressure and molecular mobility. The use of finer NMR experimental procedures (for example, experiments under different temperatures and pressures, measuring the T_1 spectrum, T_2 spectrum, D - T_2 two-dimensional spectrum, respectively, etc.) is indeed

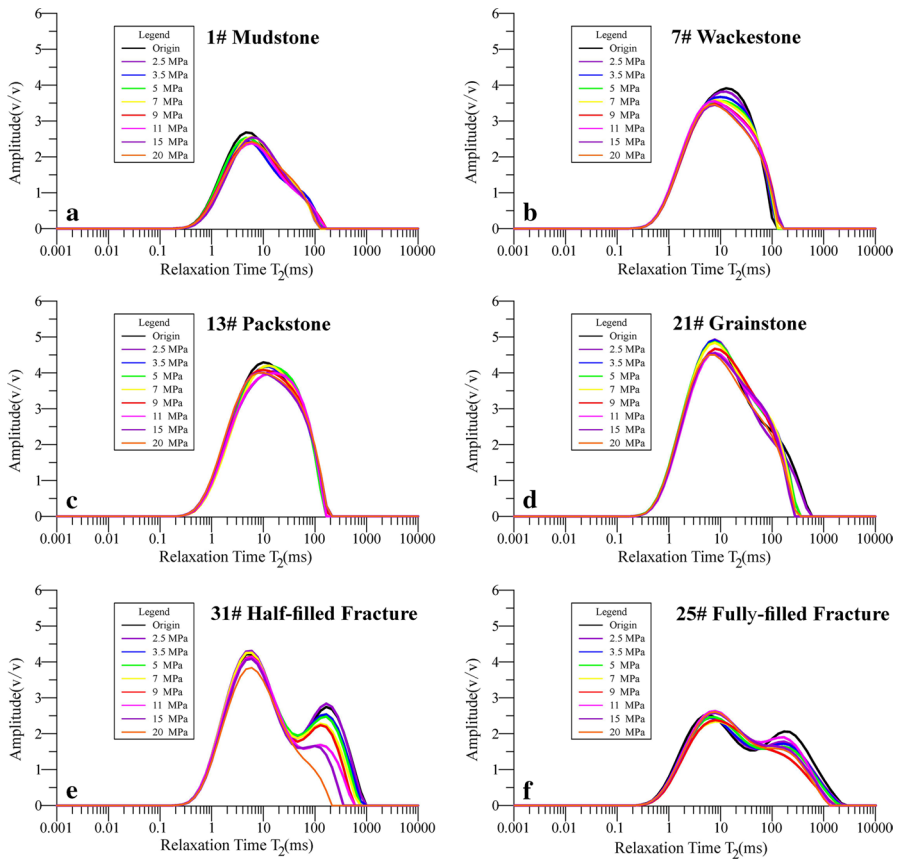


Fig. 6 The NMR T_2 distributions of each rock type under different pressures (up to 20 MPa). **a** Mudstone, **b** wackestone, **c** packstone, **d** grainstone, **e** limestone with half-filled fractures, **f** limestone with fully filled fractures

possible to obtain more accurate information on the pore structure of rock samples. In account of the practicality, due to the short measurement time of T_2 measurement (in a matter of minutes), the oil industry generally measures T_2 spectra to indirectly characterize the different sizes of pore structures in rocks, both in experimental measurements and field NMR logging [28–30].

4.1 Comparison of the MICP and NMR pore structure results

The MICP curve shape is controlled by the pore throat system of the tested cylinder. Hence, the MICP curves reflect the storage space and can be used to calculate the rock pore throat radius distribution and average pore throat radius [31]. The limitations of the MICP technique are also obvious: the transport media is poisonous mercury, the measurements include human error, the measurement period is long

and, therefore, costly, and MICP analysis permanently damages the samples. Therefore, MICP tests are not appropriate for numerous core samples. Using a sample of hydrogen atoms and their magnetic resonance to generate signal characteristics, NMR experiments can detect the fluid in the pore network. NMR is convenient, quick, and simple to operate; does not involve pollution; and can be used to analyze numerous core samples. More importantly, the results of NMR experiments can be linked to the results of MICP experiments.

The following relationship between capillary pressure and pore diameter is obtained:

$$P_C = \frac{2\sigma \cos \theta}{r_c}. \quad (1.4)$$

In this equation, P_C is capillary pressure, MPa; σ is fluid interface tension, N/cm²; θ is wetting contact angle, °; r_c is the capillary radius, μm .

For mercury, $\sigma = 49.44 \text{ N/cm}^2$ and $\theta = 140^\circ$; hence, the equation can be rewritten as follows:

$$P_C = \frac{0.735}{r_c} \quad (1.5)$$

Combining this equation with Eq. 1.3 produces the following:

$$\frac{0.735}{P_C} = \rho_2 \times F_S \times T_2 \quad (1.6)$$

$$P_C = C \times \frac{0.735}{T_2} \quad (1.7)$$

In Eq. 1.7, $C = \frac{1}{\rho_2 \times F_S}$ is called the conversion coefficient.

With a known MICP curve, the T_2 distribution can be approximated, producing a so-called pseudo T_2 distribution. With the T_2 distribution, the MICP curve can also be approximated, producing a so-called pseudo capillary pressure curve.

Carbonate rocks are complex objects. Getting a satisfactory agreement between the results of NMR and MICP is very important for pore structure characterization. As an indirect measurement method to characterize rock pore structures, the NMR results must be calibrated by pore structure distributions which were obtained from MICP. The conversion coefficient (C) is a linkage between results of NMR and MICP. Due to the inherent strong heterogeneity of carbonate rocks, we classified six rock types based on geological observations. Because the rocks in the same rock type have similar pore structures, while the rocks in different rock types have obviously different pore structures, we matched the results of NMR and MICP according to their own rock types with different C value, respectively (Table 3), and got a satisfactory agreement between the results of NMR and MICP.

Table 3 The *C* value of each rock type

Rock type	Mudstone	Wackestone	Packstone	Grainstone	Limestone with half-filled fractures	Limestone with fully-filled fractures
<i>C</i> value	895	967	985	1831	852.1	615.3

In this study, we found that the tight carbonate pore structure results based on NMR experiments closely matched those based on the MICP curves after the rock typing. Both pore structure results for mudstone feature a unimodal pattern and are consistent with each other in terms of amplitude (Fig. 7a); hence, the pore throat system characterizations of the NMR and MICP methods are consistent. For tight carbonate wackestone, packstone and grainstone, there are some slight differences in the pore structure results of the MICP and NMR methods: the throat volume percentage from the MICP experiments is significantly greater than that from the NMR experiments (Fig. 7b–d). This difference occurs because the main measurement of the mercury injection process is the pore throat breakthrough pressure, and some of the pores connected to pore throats are calculated as the throat volume [32]. The MICP results reflect the connected pores, while the NMR results reflect the total pore space saturated with water. Hence, the pore volume of the tested tight carbonate cylinder is slightly larger in the NMR results than in the MICP results. In the grainstone (Fig. 7d) and fractured limestone (Fig. 7e, f), the pore structure

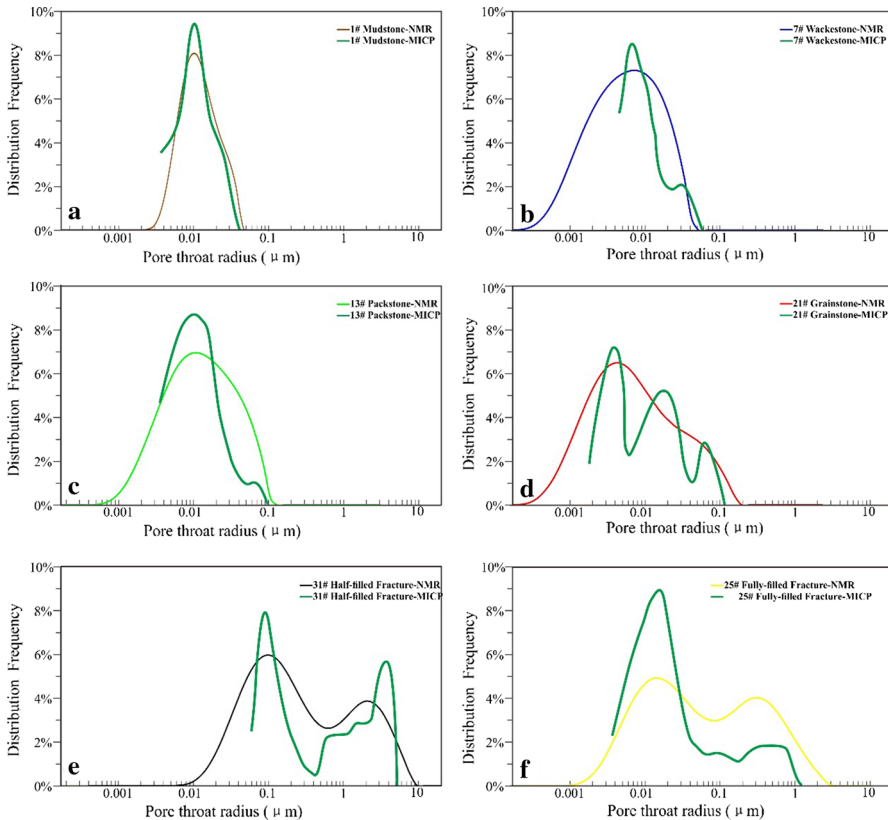


Fig. 7 The pore structure distributions from the MICP and NMR experiments for the six rock types. **a** Mudstone, **b** wackestone, **c** packstone, **d** grainstone, **e** limestone with half-filled fractures, **f** limestone with fully filled fractures

measurements via NMR and MICP are broadly similar, but due to the complexity of the pore structure of the tight carbonate rock, the MICP pore structure results are not very continuous, even with numerous test points, whereas the NMR pore structure has a continuous and smooth pore size distribution curve.

4.2 Pore Compaction Under Pressure

In the process of the MICP tests, the pore volume was compacted under different pressures, whereas during the NMR experiments, the cylinders were under normal atmospheric pressure. We believe that this is a key factor in the differences in the pore structure results between the NMR and MICP experiments, which has been neglected so far. In deeply buried strata and tight carbonate rocks, the differences must be considered. Furthermore, the NMR T_2 spectrum measured under atmospheric pressure may be different than subsurface measurements.

The NMR online test system used in this paper can detect pore changes at pressures less than 20 MPa, which can provide references for in situ pore structure analysis in the subsurface. By calculating the rate of change in the volume, we found that the volumetric compression of different rock phases varies. Mud-supported carbonate rocks compress little under high pressure, and the volume at 20 MPa relative to that at atmospheric pressure is 89.03–95.96% (Fig. 8). In contrast, grain-supported limestone compresses relatively easily, e.g., the compressed volume of the grainstone was 77.61% at 20 MPa. The fractured limestone exhibited clear volumetric compression, especially the half-filled fractures, which were compressed to 62.14% at 20 MPa. Therefore, volumetric compression under different pressure conditions needs to be considered because this compression may be an influential factor in the differences in the pore structure results of the MICP and NMR measurements.

5 Conclusions

- (1) Based on geological observations of the 25 core samples and related thin sections, the Dunham classification and fracture development, six rock types were identified in this study: mudstone, wackestone, packstone, grainstone, limestone with fully filled fractures, and limestone with half-filled fractures. We found that the thick grainstone and limestone with half-filled fractures represented good potential reservoirs.
- (2) Carbonate rocks are complex objects. Due to the inherent strong heterogeneity of carbonate rocks, getting a satisfactory agreement between the results of NMR and MICP is very important for pore structure characterization. A series of comparisons between the T_2 pore network and mercury injection capillary pressure (MICP) pore network were analyzed for each rock type, and the results of the two methods are consistent. We can analyze numerous core samples conveniently, quickly, and without damage, using the NMR testing method.

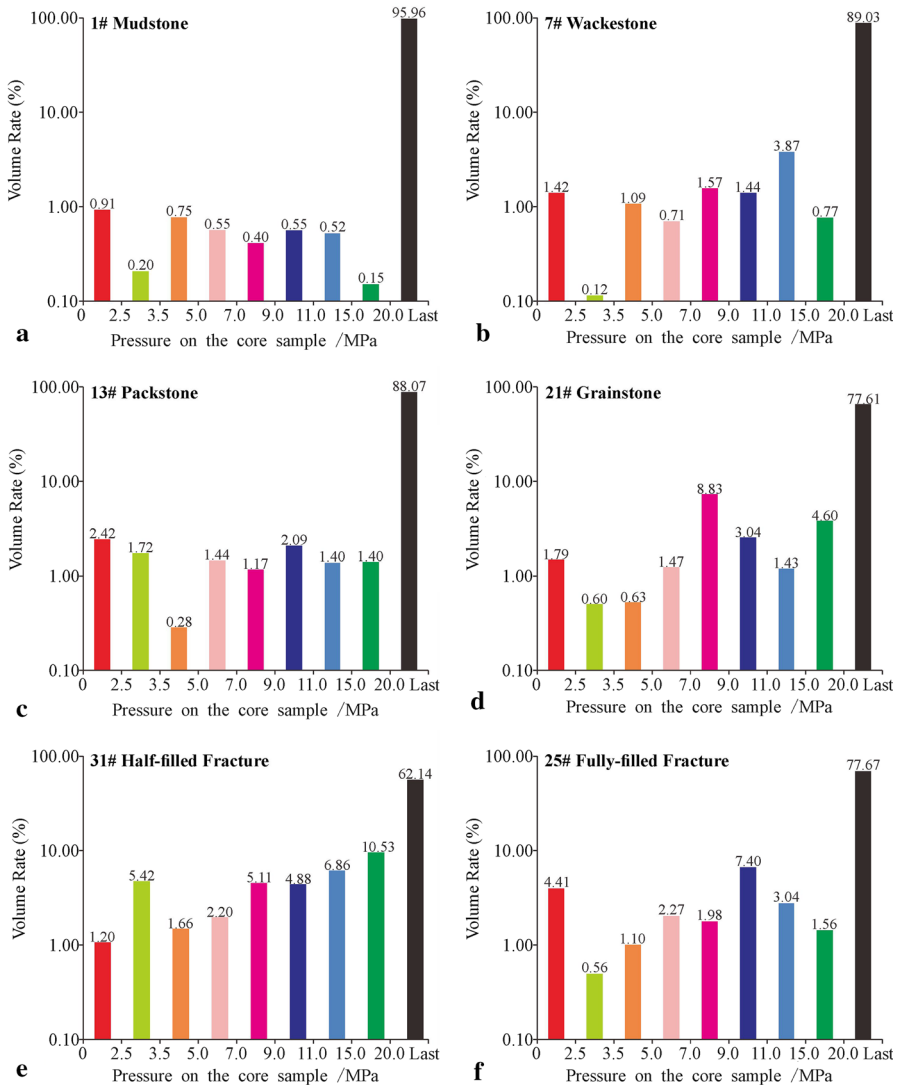


Fig. 8 Pore compaction of each rock type under different pressures. **a** Mudstone, **b** wackestone, **c** packstone, **d** grainstone, **e** limestone with half-filled fractures, **f** limestone with fully filled fractures

(3) Using the overburden pressure NMR online test system, the pore structures of the six rock types were analyzed at atmospheric pressure and at 20 MPa. We found that the micropore-dominated mudstone and wackestone are more resistant to compaction (volumetric compression of approximately 10%). The packstone and grainstone, which contain mesopores and macropores, exhibit greater compaction (volumetric compression of approximately 10–25%). The

fractured limestone can be significantly compacted (volumetric compression of approximately 25–45%).

Acknowledgements This study was supported by National Basic Research Program of China (973 Program, Grant No. 2015CB250902), the Strategic Priority Research Program of the Chinese Academy of Sciences (Grant No. XDA14040404), the Chinese National Major Fundamental Research Developing Project (Grant No. 2017ZX05008-004), the Chinese National Natural Science Foundation (Grant Nos. 41502149, and U1663204) and the China Postdoctoral Foundation Funded Project (Grant No. 2015M570148). We are deeply grateful to the Tahe Oilfield Branch Company SINOPEC for supplying the data and allowing this paper to be published. We thank two anonymous reviewers for their thorough and critical reviews and suggestions, which have improved the manuscript.

References

1. C. Rühl, BP statistical review of world energy 2007. ©BP (2007)
2. W. Zhao, S. Hu, L. Wei, T. Wang, Y. Li, *Nat. Gas Ind.* **1**, 14–23 (2014)
3. G.Y. Zhu, M. Wang, T.W. Zhang, Identification of polycyclic sulfides hexahydrodibenzothiophenes and their implications for heavy oil accumulation in ultra-deep strata in Tarim Basin. *Mar. Pet. Geol.* **78**, 439–447 (2016)
4. F. Tian, Q. Jin, X. Lu, Y. Lei, L. Zhang, S. Zhang, *Mar. Pet. Geol.* **69**(1), 53–73 (2016)
5. X. Lu, Y. Wang, F. Tian, X. Li, D. Yang, T. Li, *Mar. Pet. Geol.* **86**, 587–605 (2017)
6. H. Zeng, R. Loucks, X. Janson, G. Wang, Y. Xia, B. Yuan, *AAPG Bull.* **95**(12), 2061–2083 (2011)
7. S.Z. Sun, Z. Liu, N. Dong, Y. Zhang, L. Yu, P. Wang, in *Society of Exploration Geophysicists Annual Meeting* (New Orleans, USA, 18–23 October 2015), p. 2821–2825
8. Q. Jin, F. Tian, *J. Chin. Univ. Pet.* **37**, 515–521 (2013)
9. Q. Jin, F. Tian, H. Zhang, *Acta Pet. Sin.* **36**(7), 791–798 (2015)
10. A.R. Adebayo, M.E. Kandil, T.M. Okasha, M.L. Sanni, *Int. J. Greenhouse Gas Control* **63**, 1–11 (2017)
11. G. Mariappan, N. Sundaraganesan, *Spectrochim Acta A* **110**(6), 169–178 (2013)
12. X. Ge, Y. Fan, Y. Cao, *Appl. Magn. Reson.* **45**(2), 155–167 (2014)
13. M. Claverie, C. Reynaud, in *SPE Europec Featured at 78th EAGE Conference and Exhibition* (Vienna, Austria, 30 May–2 June 2016), SPE-180182-MS
14. F. Deng, L. Xiao, M. Wang, *Appl. Magn. Reson.* **47**(11), 1–15 (2016)
15. U. Farooq, R. Iskandar, E.S.M. Radwan, M.A.H. Hozayen, in *Abu Dhabi International Petroleum Exhibition and Conference* (Abu Dhabi, UAE, 10–13 November, 2014), SPE-171932-MS
16. Y. Li, in *Society of Exploration Geophysicists Rock Physics & Borehole Geophysics Workshop* (Beijing, China, 28–30 August, 2016), p. 56–59
17. B. Vik, K.E. Sylta, A. Skauge, *Transp. Porous Media* **93**(3), 561 (2012)
18. M.F. Rezende, S.N. Tonietto, M.C. Pope, *AAPG Bull.* **97**(11), 2085–2101 (2013)
19. Z.L. He, S.T. Peng, T. Zhang, *Oil Gas Geol.* **31**(6), 743–752 (2010)
20. F. Tian, X. Lu, S. Zheng, H. Zhang, Y. Rong, D. Yang, *Open Geosci.* **9**, 266–280 (2017)
21. T.A. Cheema, C.Y. Lee, G.M. Kim, J.G. Hong, M.K. Kwak, C.W. Park, *Int. J. Precis. Eng. Manuf.* **15**(7), 1405–1410 (2014)
22. O. Fay-Gomord, J. Soete, K. Katika, S. Galaup, B. Caline, F. Descamps, *Mar. Pet. Geol.* **75**, 252–271 (2016)
23. E. Grunewald, R. Knight, *Geophysics* **74**, 215–221 (2009)
24. W.E. Kenyon, *Soc. Petrophys. Well Log Anal.* **38**, 21–43 (1997)
25. B. Vincent, M. Fleury, Y. Santerre, B. Brigaut, NMR relaxation of neritic carbonates: an integrated petrophysical and petrographical approach. *J. Appl. Geophys.* **74**, 38–58 (2011)
26. X.M. Ge, Y.R. Fan, Y.F. Xiao, J.Y. Liu, D.H. Xing, D.N. Gu, S.G. Deng, Quantitative evaluation of the heterogeneity for tight sand based on the nuclear magnetic resonance imaging. *J. Nat. Gas Sci. Eng.* **38**, 74–80 (2017)
27. R.J. Dunham, *Classif. Carbonate Rocks* **1**, 108–121 (1962)

28. F.F. Wang, T.Z. Tang, T.Y. Liu, H.N. Zhang, *Appl. Magn. Reson.* **47**(4), 1–13 (2016)
29. M. Liu, R. Xie, C. Li, L. Gao, *Appl. Magn. Reson.* **48**(4), 1–21 (2017)
30. Z. Yang, Y. Zhang, H. Li, X. Zheng, Q. Lei, *Earth Sci.* **42**(8), 1333–1339 (2017)
31. F. Rashid, P.W.J. Glover, P. Lorinczi, D. Hussein, R. Collier, J. Lawrence, Permeability prediction in tight carbonate rocks using capillary pressure measurements. *Mar. Pet. Geol.* **68**, 536–550 (2015)
32. X.M. Ge, Y.R. Fan, J.T. Li, M.A. Zahid, Pore structure characterization and classification using multifractal theory—An application in Santanghu basin of western China. *J. Pet. Sci. Eng.* **127**, 297–304 (2015)